MAGNONICS

Magnetization switching by magnon-mediated spin torque through an antiferromagnetic insulator

Yi Wang[1,2]*, Dapeng Zhu[1]*, Yumeng Yang[1], Kyusup Lee[1], Rahul Mishra[1], Gyungchoon Go[3], Se-Hyeok Oh[4], Dong-Hyun Kim[5], Kaiming Cai[1], Enlong Liu[1], Shawn D. Pollard[1], Shuyuan Shi[1], Jongmin Lee[1], Kie Leong Teo[1], Yihong Wu[1], Kyung-Jin Lee[3,4,5,6], Hyunsoo Yang[1]†

Widespread applications of magnetic devices require an efficient means to manipulate the local magnetization. One mechanism is the electrical spin-transfer torque associated with electron-mediated spin currents; however, this suffers from substantial energy dissipation caused by Joule heating. We experimentally demonstrated an alternative approach based on magnon currents and achieved magnon-torque–induced magnetization switching in Bi_2Se_3/antiferromagnetic insulator NiO/ferromagnet devices at room temperature. The magnon currents carry spin angular momentum efficiently without involving moving electrons through a 25-nanometer-thick NiO layer. The magnon torque is sufficient to control the magnetization, which is comparable with previously observed electrical spin torque ratios. This research, which is relevant to the energy-efficient control of spintronic devices, will invigorate magnon-based memory and logic devices.

Spin current, a flow of spin angular momentum, is the essential ingredient for spin-transfer torque. One class of spin currents is the electrical spin current J_S, which is associated with electron spins (*1*–*3*). When J_S is absorbed by a magnet, the magnetization experiences an electrical spin torque, and its direction is reoriented (Fig. 1A). The electrical spin torque has opened the era for electrically controlled magnetic device applications—for example, magnetic random access memories (*3*). However, J_S is commonly associated with charge flow so that Joule heat and corresponding power dissipation are unavoidable. Moreover, the spin propagation length (diffusion length) of J_S is relatively short, typically on the order of nanometers (*4*), which prevents the delivery of spin information over long distances.

These limitations could be overcome by another class of spin currents, the magnon current J_M, for which the spin angular momentum is carried by precessing spin moments rather than moving electrons (*5*). The magnon torque associated with J_M shows several advantages in comparison with the electrical spin torque. There is no electron movement in J_M; therefore, much less Joule heat dissipation is expected. Moreover, J_M can flow even in insulators for distances up to several micrometers (*6*–*9*), and thus, material systems for the magnon torque are not limited to electrical conductors. As J_M approaches a magnet, it interacts with the magnetization through the exchange coupling, and consequently, the magnetization can be reoriented by the magnon torque (Fig. 1B). However, most studies on magnon currents have focused on long-distance transport (*6*–*9*), whereas experimental works on magnon-mediated spin torques (*10*–*13*) have been limited to magnetic excitations or thermally driven domain wall motion (*14*–*16*), and the magnetization switching has been realized only by the electrical spin torque. In this work, we observed a giant magnon torque with a ratio for the J_M generation of ~0.3, which is comparable with the electrical spin torque ratio of topological insulators (*17*–*19*), and we experimentally demonstrated that the magnetization can be efficiently switched by the magnon torque without any external magnetic field at room temperature.

We fabricated Bi_2Se_3 (8 nm)/NiO (t_{NiO} = 0 to 100 nm)/NiFe (Py, 6 nm) structures, where t_{NiO} is the thickness of NiO, with the Bi_2Se_3 (fig. S1 and materials and methods) (*20*) acting as a highly efficient spin current source (*17*–*19*). In-plane current injection to the Bi_2Se_3 produces electrical spin currents at the Bi_2Se_3/NiO interface and excites J_M in the NiO layer. We chose NiO, an antiferromagnetic insulator, as a magnon-current medium because magnons are the sole spin angular momentum carriers (*6*–*9*, *21*–*24*) in the NiO layer.

Because antiferromagnetic ordering has a crucial role in magnon transport through antiferromagnets (*25*), we first characterized the thickness dependence of the antiferromagnetic ordering in the NiO layer by measuring hysteresis loops. The antiferromagnetic ordering can be estimated by the exchange bias field or coercivity; both increase as the antiferromagnetic ordering improves (*26*). The temperature-dependent exchange bias field H_{ex} of Bi_2Se_3/NiO/Py is shown in Fig. 2A for various t_{NiO}. H_{ex} increases with the NiO thickness at $t_{NiO} \leq 25$ nm at 2 K. The blocking temperature T_b, at which the H_{ex} becomes zero, increases as t_{NiO} increases (Fig. 2B). A similar trend is observed for the coercivity H_c at room temperature (Fig. 2C); H_c increases with t_{NiO} for $t_{NiO} \leq 30$ nm. H_c then slightly decreases with increasing t_{NiO}, which is a typical behavior of antiferromagnetic films. The results suggest that the antiferromagnetic ordering in the NiO layer gradually improves as t_{NiO} increases. The smaller T_b than that in NiO bulk (Fig. 2B) is related to the polycrystalline structure of NiO grown on Bi_2Se_3 (Fig. 2D). When the NiO layer is directly deposited on the c-plane sapphire substrate, it shows a good crystallinity with the dominant (111) plane. However, when the NiO layer is deposited on Bi_2Se_3, it is polycrystalline, possibly because of the lattice mismatch between the NiO and Bi_2Se_3 layers.

We next characterized the magnon torque using the spin torque ferromagnetic resonance (ST-FMR) measurement (Fig. 3A) (*17*, *20*, *27*, *28*). A radio frequency current (I_{RF}; current density J_C in the Bi_2Se_3 layer) was applied to the device and generated electrical spin currents with a spin polarization denoted in Fig. 3A with a red arrow at the Bi_2Se_3/NiO interface. J_M is then induced in the NiO layer through the exchange interaction between the spins and nearby NiO moments (*29*). Passing through the NiO layer, J_M exerts a magnon torque on the Py layer. Consequently, the Py magnetization is excited into the precession mode, generating a ST-FMR signal V_{mix}. V_{mix} (Fig. 3B, open symbols) from a representative device with t_{NiO} = 25 nm is fitted by $V_{mix} = V_S F_S + V_A F_A$, where $V_S F_S$ and $V_A F_A$ are the symmetric and antisymmetric components, respectively. By adopting an established analysis method (*17*, *20*, *27*), we evaluated the spin torque ratio ($\theta_i = J_i/J_C$) for the symmetric component, which is analogous to the spin Hall angle in the electrical spin-orbit torque scheme (*17*, *27*). θ_i is caused either by the electrical spin torque (stemming from J_S, i = S) or by the magnon torque (stemming from J_M, i = M), depending on the NiO thickness, which is discussed later.

Shown in Fig. 3C is θ_i versus t_{NiO} at room temperature, at which the NiO/Py interface contribution is subtracted [fig. S2 and (*20*), section 2]. For the device without the NiO layer—the Bi_2Se_3/Py bilayer—θ_i is 0.67, which is consistent with a previous report for Bi_2Se_3 (*18*). We observed that θ_i abruptly decreases from 0.67 to ~0 by inserting only a 2-nm NiO layer between the Bi_2Se_3 and Py layers. In this NiO-thickness range, no noticeable exchange

[1]Department of Electrical and Computer Engineering, National University of Singapore, 117576, Singapore. [2]Key Laboratory of Materials Modification by Laser, Ion and Electron Beams (Ministry of Education), Dalian University of Technology, Dalian 116024, China. [3]Department of Materials Science and Engineering, Korea University, Seoul 02841, Korea. [4]Department of Nano-Semiconductor and Engineering, Korea University, Seoul 02841, Korea. [5]Department of Semiconductor Systems Engineering, Korea University, Seoul 02841, Korea. [6]KU-KIST Graduate School of Converging Science and Technology, Korea University, Seoul 02841, Korea.
*These authors contributed equally to this work.
†Corresponding author. Email: eleyang@nus.edu.sg

bias nor enhanced coercivity was observed, even at low temperature (Fig. 2). It indicates that the antiferromagnetic ordering is weak, and corresponding magnon torque has a negligible role in this thickness range. Therefore, the small θ_i would be of purely electrical origin—electron spin tunneling through a normal insulator such as MgO or SiO_2 (*21*, *22*).

The presence of magnon torque is evident for larger values of NiO thickness in which magnons are the only spin-angular-momentum carriers. We found that θ_i starts to increase as t_{NiO} increases above 10 nm (Fig. 3C). θ_i shows a peak value of ~0.3 at t_{NiO} = 25 nm and then gradually decreases with further increasing t_{NiO} up to 100 nm. The peak θ_i value is of similar magnitude to the electrical spin Hall angle of topological insulators (*17*–*19*) and is higher than that of heavy metals Pt and Ta (*30*).

We used independent terahertz emission measurements to double check the NiO thickness–dependent behavior [fig. S3 and (*20*), section 3]. The terahertz emission amplitude characterizes the spin-to-charge conversion, which is the reciprocal process of the ST-FMR measurements (charge-to-spin) (*31*, *32*). A similar trend in Fig. 3C by using both ST-FMR and terahertz techniques validates our observations of NiO thickness–dependent magnon torques. As a control experiment, we inserted a 6-nm MgO layer between Bi_2Se_3 and NiO layers to block the spins through the NiO layer (*33*), and the obtained θ_i is negligible (Fig. 3C, star symbol). This rules out the possibility that observed torque is generated at the NiO/Py interface [table S1 and (*20*), section 4]. The temperature dependence of θ_i measured for Bi_2Se_3/NiO (t_{NiO} = 2, 5 and 25 nm)/NiFe devices is shown in Fig. 3D. The θ_i shows a peak at a certain temperature close to the antiferromagnetic transition in the NiO layer for each device, at which the enhanced spin fluctuations and magnons facilitate the spin transport, which is in line with the previous reports (*23*, *24*, *34*, *35*). These results confirm the magnon-originated nature of the spin torque.

To gain insight into the thickness dependence of θ_i, we estimated a transverse magnon current at the NiO/Py interface using a simple drift-diffusion model. Because the NiO layer is polycrystalline (Fig. 2D), we assumed that magnon propagation in the NiO layer is diffusive (*25*, *36*). In this model, the resultant transverse magnon current $J_m^{\perp}$ at the NiO/Py interface is

$$J_m^{\perp} = \theta_i J_C = \eta\theta J_C \frac{2G_{A/F}^{\perp} l_m \kappa}{G_{A/F}^{\perp} l_m (1+\kappa^2) + 2\pi\sigma_m (1-\kappa^2)} \quad (1)$$

where θ is the spin Hall angle of Bi_2Se_3 layer; η is the angular momentum loss at the Bi_2Se_3/NiO interface; $G_{A/F}^{\perp}$ is the interfacial magnon conductance for the transverse component between NiO and Py (*36*), which is analogous to the mixing conductance of the spin transport theory (*37*); $\kappa = \exp(-t_{NiO}/l_m)$; and l_m and σ_m are the magnon diffusion length and magnon conductivity of the NiO layer, respectively [(*20*), section 5]. The red curve in Fig. 3C is the fit of experimental data to Eq. 1. For the fitting, we assumed that l_m increases with t_{NiO} and saturates at ~30 nm (Fig. 3C, inset); the value of 30 nm was estimated from the exponential decrease of θ_i for $t_{NiO} \geq 25$ nm in Fig. 3C; the saturation l_m of ~30 nm is consistent with that recently reported in polycrystalline NiO (*38*). This assumption is motivated by the experimental results shown in Fig. 2; the behaviors of H_{ex} (or T_b) and H_c with t_{NiO} suggest an improvement of antiferromagnetic ordering with t_{NiO}. To support this assumption, we performed atomistic lattice spin model calculations for the relation between the antiferromagnetic ordering and l_m and found that they are correlated (fig. S5). The reasonable fit shown in Fig. 3C implies that the t_{NiO}-dependent change

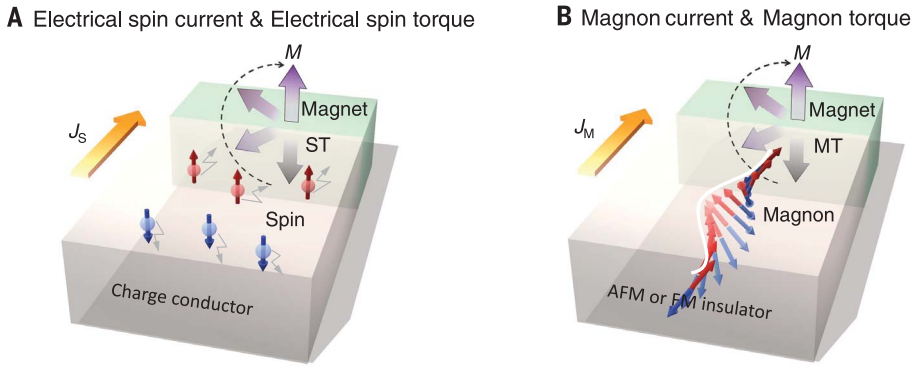

Fig. 1. Two types of spin-angular-momentum-transfer torque. (**A**) Illustration of the magnetization (*M*) reorientation driven by the electrical spin torque (ST) by means of the electrical spin current J_S. (**B**) Illustration of the magnetization (*M*) reorientation driven by the magnon torque (MT) by means of the magnon current J_M. AFM, antiferromagnet; FM, ferromagnet.

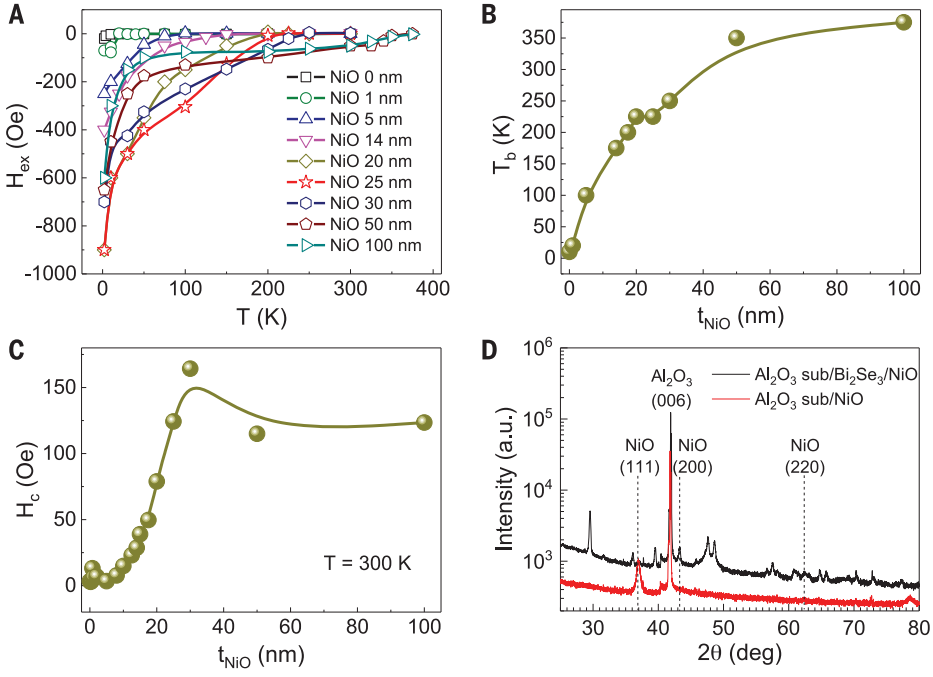

Fig. 2. Characterization of Bi_2Se_3/NiO/Py structures. (**A**) The exchange bias as a function of temperature for various NiO thicknesses (t_{NiO}). (**B**) The blocking temperature deduced from (A). (**C**) The coercivity as a function of t_{NiO} at room temperature. (**D**) X-ray diffraction patterns of sapphire substrate/Bi_2Se_3 (8 nm)/NiO (100 nm) and sapphire substrate/NiO (100 nm).

of l_m is a possible explanation for the experimental observation, even though a more detailed study is required for a quantitative understanding.

Last, we demonstrated magnetization switching induced by the magnon torque in the Bi_2Se_3/NiO/Py heterostructure at room temperature (Fig. 4). In switching devices, the Py layer was patterned into a rectangular shaped island to prohibit current shunting through the Py layer (Fig. 4, A and B) (*20*). The switching results for t_{NiO} = 25 nm are shown in Fig. 4, C to F, measured with a magneto-optic Kerr effect (MOKE) microscope by injecting a pulsed current *I*. We first saturated the magnetization in the Py island (Fig. 4C, yellow box) along the +*y* axis with an in-plane magnetic field. Then, we removed the field and applied *I* (J_C ~ 1.27 × 10^7 A cm^{-2}) along the +*x* axis. We found that the Py magnetization was switched to the –*y* axis, indicated by the contrast change from dark to light in the yellow box (Fig. 4D). We then initialized the Py magnetization along the –*y* axis (Fig. 4E) and applied *I* (J_C ~ –1.27 × 10^7 A cm^{-2}) along the –*x* axis. The Py magnetization was switched to the +*y* axis (Fig. 4F). This bidirectional switching depending on the current polarity excludes the possibility that the switching is governed by Joule heating–induced effects. This magnon torque–driven magnetization switching is reproducible in other devices (fig. S6). We also demonstrated magnetization switching induced by magnon torques in Bi_2Se_3/NiO (25 nm)/$Co_{40}Fe_{40}B_{20}$ (CoFeB) trilayers at room temperature (fig. S7).

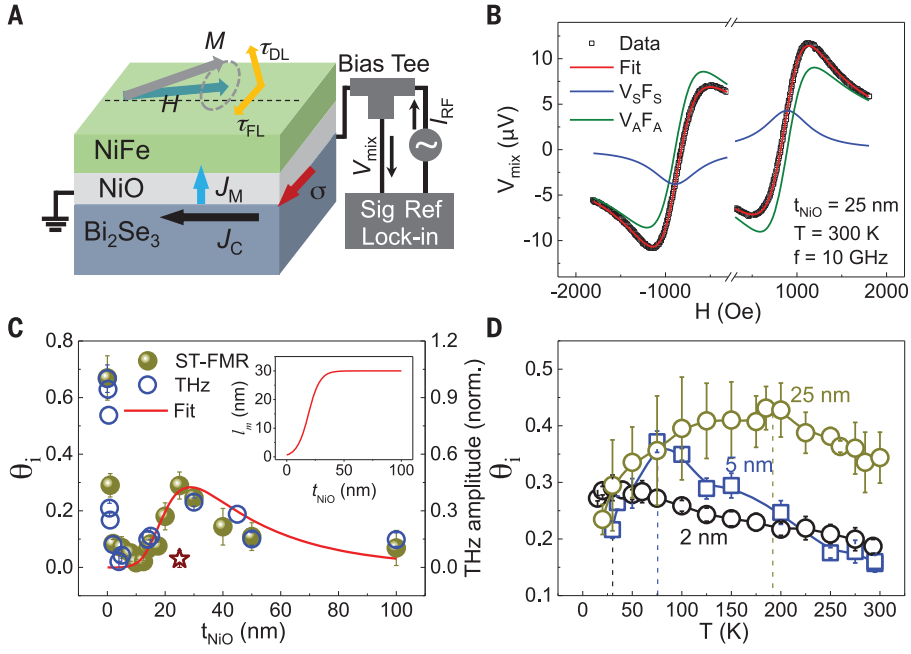

Fig. 3. ST-FMR measurement of magnon torque. (**A**) A diagram of the ST-FMR measurements, illustrating the magnetization precession driven by the spin torque, including the damping-like torque τ_{DL} and/or field-like torque τ_{FL}. The black arrow denotes the direction of I_{RF} with a current density J_C. The red and blue arrows indicate spin polarizations and magnon current J_M, respectively. (**B**) A typical ST-FMR signal (open symbols) from a Bi_2Se_3/NiO (25 nm)/Py (6 nm) device at 10 GHz and 300 K with fits (solid lines), where the blue and green lines indicate the symmetric (V_SF_S) and antisymmetric Lorentzian (V_AF_A) component, respectively. (**C**) The spin torque ratio θ_i deduced from the ST-FMR data (solid circles) and the terahertz emission amplitude (open circles) as a function of t_{NiO} at 300 K. The red curve is a fit using Eq. 1. For the fitting, we used $\eta\theta$ = 0.8 and $G^{\perp}_{A/F}/\sigma_m = 3 \times 10^8$ m^{-1}. (Inset) The assumed magnon diffusion length (l_m) as a function of t_{NiO}. The star symbol corresponds to θ_i obtained from the ST-FMR measurement of the control device with 6-nm MgO insertion between Bi_2Se_3 and NiO layers. (**D**) Temperature dependence of θ_i for Bi_2Se_3/NiO (t_{NiO} = 2, 5, and 25 nm)/Py (6 nm) devices.

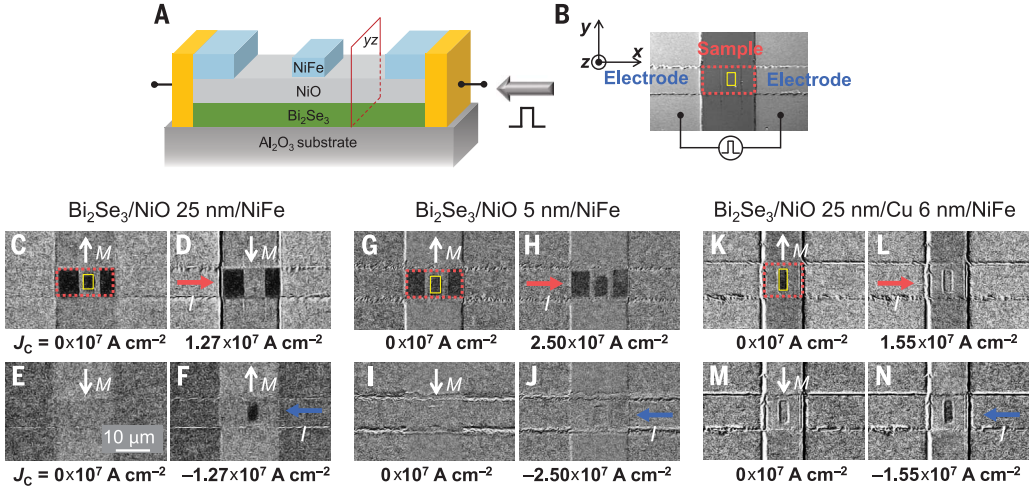

Fig. 4. Magnetization switching induced by magnon torque in the Bi_2Se_3/NiO/Py devices at room temperature. (**A**) Illustration of the structure of the magnon torque switching device with an isolated Py rectangle defined on top of the NiO layer. (**B**) Optical microscope image of a device with electrodes, where the sample functional region is indicated with a red dotted box and an isolated Py rectangle is denoted with a yellow box. (**C** to **F**) MOKE images for magnon-torque-driven magnetization switching in the Bi_2Se_3/NiO (25 nm)/Py device by injecting a pulsed current *I* along the [(C) and (D)] +*x* axis or [(E) and (F)] –*x* axis at room temperature. (**G** to **J**) MOKE images for a Bi_2Se_3/NiO (5 nm)/Py device by injecting *I* along the [(G) and (H)] +*x* axis or [(I) and (J)] –*x* axis at room temperature. (**K** to **N**) MOKE images for the Bi_2Se_3/NiO (25 nm)/Cu (6 nm)/Py device by injecting *I* along the [(K) and (L)] +*x* axis or [(M) and (N)] –*x* axis at room temperature. In (C) to (N), the dark contrast represents the magnetization along the +*y* axis, and the light contrast represents the magnetization along the –*y* axis. The direction of magnetization is indicated with white arrows. The current density J_C in the Bi_2Se_3 layer is denoted underneath each image.

The switching experiments on another device of Bi_2Se_3/NiO (5 nm)/Py are shown in Fig. 4, G to J, in which θ_i estimated from ST-FMR is negligible (Fig. 3C). Following the same measurement procedures as in Fig. 4, C to F, we could not observe the magnetization switching, even with a larger J_C. This behavior was reproducible in other devices with t_{NiO} = 5 nm. It excludes a possibility that the current-induced Oersted field, which is also present in the devices with t_{NiO} = 5 nm, is the origin of the magnetization switching observed in the devices with t_{NiO} = 25 nm. We also performed switching experiments on other devices with isolated Py islands at various t_{NiO} and found that the switching efficiency is qualitatively consistent with θ_i estimated from ST-FMR (fig. S9). Therefore, our results provide unambiguous evidence that the switching is governed by the magnon torque.

From the above experiments, one question is whether direct exchange coupling between NiO and Py magnetic moments is essential for large magnon torques or not. To answer this, we performed switching experiments in Bi_2Se_3/NiO (25 nm)/Cu (6 nm)/Py devices, in which the Cu layer breaks direct exchange coupling but allows spin transmission through the transfer of spin angular momentum from magnons to electrons (Fig. 4, K to N). Both the Py and Cu insertion layer were patterned into a rectangular shaped island to eliminate current shunting through the Cu/Py bilayer. Following the same measurement procedures as in Fig. 4, C to F, we observed robust magnetization switching with $J_C \sim 1.55 \times 10^7$ A cm^{-2}, which was reproducible in other devices with a Cu insertion (fig. S8). The observations confirm that direct exchange coupling between the NiO and Py magnetic moments is not essential for the magnon torque–induced magnetization switching.

Our demonstration reveals the ability of magnon torque to switch magnetization, a process that is as energy efficient as electrical spin torques. This research will broaden the scope of not only magnon-related studies that are mainly focused on magnon transport (*6–9*, *21–24*, *39*) but also spintronics studies, in which advances have relied largely on the electrical spin torque. In this study, we induced the magnon torque in an antiferromagnetic insulator by injecting the electric current to a Bi_2Se_3 layer as a proof of principle. However, our work is just a starting point to explore the magnon torque–driven magnetization switching. We expect that all-magnon-driven magnetization switching, without involving electrical parts, could be achieved in the near future.

REFERENCES AND NOTES

1. J. C. Slonczewski, *J. Magn. Magn. Mater.* **159**, L1–L7 (1996).
2. L. Berger, *Phys. Rev. B* **54**, 9353–9358 (1996).
3. A. Brataas, A. D. Kent, H. Ohno, *Nat. Mater.* **11**, 372–381 (2012).
4. J. Bass, W. P. Pratt Jr., *J. Phys. Condens. Matter* **19**, 183201 (2007).
5. A. Chumak, V. Vasyuchka, A. Serga, B. Hillebrands, *Nat. Phys.* **11**, 453–461 (2015).
6. Y. Kajiwara *et al*., *Nature* **464**, 262–266 (2010).
7. L. Cornelissen, J. Liu, R. Duine, J. B. Youssef, B. Van Wees, *Nat. Phys.* **11**, 1022–1026 (2015).
8. W. Yuan *et al*., *Sci. Adv.* **4**, eaat1098 (2018).
9. R. Lebrun *et al*., *Nature* **561**, 222–225 (2018).
10. J. C. Slonczewski, *Phys. Rev. B* **82**, 054403 (2010).
11. P. Yan, X. S. Wang, X. R. Wang, *Phys. Rev. Lett.* **107**, 177207 (2011).
12. D. Hinzke, U. Nowak, *Phys. Rev. Lett.* **107**, 027205 (2011).
13. A. A. Kovalev, Y. Tserkovnyak, *EPL* **97**, 67002 (2012) (Europhysics Letters).
14. W. Jiang *et al*., *Phys. Rev. Lett.* **110**, 177202 (2013).
15. T. Moriyama *et al*., *Appl. Phys. Lett.* **106**, 162406 (2015).
16. S. Woo, T. Delaney, G. S. Beach, *Nat. Phys.* **13**, 448–454 (2017).
17. A. R. Mellnik *et al*., *Nature* **511**, 449–451 (2014).
18. Y. Wang *et al*., *Nat. Commun.* **8**, 1364 (2017).
19. J. Han *et al*., *Phys. Rev. Lett.* **119**, 077702 (2017).
20. Materials and methods are available as supplementary materials.
21. C. Hahn *et al*., *EPL* **108**, 57005 (2014) (Europhysics Letters).
22. H. Wang, C. Du, P. C. Hammel, F. Yang, *Phys. Rev. Lett.* **113**, 097202 (2014).
23. W. Lin, K. Chen, S. Zhang, C. L. Chien, *Phys. Rev. Lett.* **116**, 186601 (2016).
24. D. Hou *et al*., *Phys. Rev. Lett.* **118**, 147202 (2017).
25. S. Rezende, R. Rodríguez-Suárez, A. Azevedo, *Phys. Rev. B* **93**, 054412 (2016).
26. J. Nogués, I. K. Schuller, *J. Magn. Magn. Mater.* **192**, 203–232 (1999).
27. Y. Wang *et al*., *Phys. Rev. Lett.* **114**, 257202 (2015).
28. Y. Wang, R. Ramaswamy, H. Yang, *J. Phys. D Appl. Phys.* **51**, 273002 (2018).
29. S. S.-L. Zhang, S. Zhang, *Phys. Rev. B* **86**, 214424 (2012).
30. A. Hoffmann, *IEEE Trans. Magn.* **49**, 5172–5193 (2013).
31. Y. Wu *et al*., *Adv. Mater.* **29**, 1603031 (2017).
32. L. Cheng *et al*., *Nat. Phys.* **15**, 347–351 (2019).
33. O. Mosendz, J. Pearson, F. Fradin, S. Bader, A. Hoffmann, *Appl. Phys. Lett.* **96**, 022502 (2010).
34. Z. Qiu *et al*., *Nat. Commun.* **7**, 12670 (2016).
35. A. Prakash, J. Brangham, F. Yang, J. P. Heremans, *Phys. Rev. B* **94**, 014427 (2016).
36. Y. Cheng, K. Chen, S. Zhang, *Appl. Phys. Lett.* **112**, 052405 (2018).
37. A. Brataas, Y. V. Nazarov, G. E. Bauer, *Phys. Rev. Lett.* **84**, 2481–2484 (2000).
38. T. Ikebuchi, T. Moriyama, H. Mizuno, K. Oda, T. Ono, *Appl. Phys. Express* **11**, 073003 (2018).
39. C. Y. Guo *et al*., *Phys. Rev. B* **98**, 134426 (2018).
40. Y. Wang *et al*., Replication Data and Code for: Magnetization switching by magnon-mediated spin torque through an antiferromagnetic insulator, Harvard Dataverse (2019); doi:10.7910/DVN/OCWIDN.

ACKNOWLEDGMENTS

We thank J. W. Yu for illustration-making assistance. **Funding:** This work was supported by SpOT-LITE program (A*STAR grant, A18A6b0057) through RIE2020 funds and the National Research Foundation (NRF), Prime Minister's Office, Singapore, under its Competitive Research Programme (CRP award NRFCRP12-2013-01). K.-J.L. was supported by the National Research Foundation of Korea (NRF-2015M3D1A1070465 and 2017R1A2B2006119) and the KIST Institutional Program (project 2V05750). Y.W. was supported by the Fundamental Research Funds for the Central Universities (project 82232016). **Author contributions:** Y.Wa. and H.Y. conceived of the research; Y.Wa., Y.Y., R.M., and K.C. fabricated the devices; D.Z., Y.Wa., and E.L. grew films; Y.Wa., S.D.P., J.L., K.L., and S.S. performed measurements; G.G. and K-J.L. contributed to the theoretical model; S.-H.O., D.-H.K., and K-J.L. performed the atomistic model calculation; Y.Wa., K-J.L. and H.Y. wrote the manuscript; all authors commented the manuscript; and H.Y. led the project. **Competing interests:** The authors declare no competing interests. **Data and materials availability:** Data reported in this paper are archived online at Harvard Dataverse (*40*).

SUPPLEMENTARY MATERIALS

science.sciencemag.org/content/366/6469/1125/suppl/DC1
Materials and Methods
Supplementary Text
Figs. S1 to S9
Table S1
References (*41–53*)

22 October 2018; resubmitted 21 August 2019
Accepted 4 November 2019
10.1126/science.aav8076

Magnetization switching by magnon-mediated spin torque through an antiferromagnetic insulator

Yi Wang, Dapeng Zhu, Yumeng Yang, Kyusup Lee, Rahul Mishra, Gyungchoon Go, Se-Hyeok Oh, Dong-Hyun Kim, Kaiming Cai, Enlong Liu, Shawn D. Pollard, Shuyuan Shi, Jongmin Lee, Kie Leong Teo, Yihong Wu, Kyung-Jin Lee and Hyunsoo Yang

Science **366** (6469), 1125-1128.
DOI: 10.1126/science.aav8076

Toward magnonic devices

The field of magnonics aims to use spin waves (SWs) and their associated quasiparticles—magnons—as carriers of information. Compared with the movement of charge in conventional electronics, a major advantage of SWs is reduced Joule heating. However, SWs are trickier to direct and control. Two groups now go a step further toward magnon-based devices. Han *et al.* show that in multilayer films, domain walls can be used to change the phase and magnitude of a spin wave. Wang *et al.* demonstrate how magnon currents can be used to switch the magnetization of an adjacent layer.

Science, this issue p. 1121, p. 1125